Proceedings of the 1999 U.S DOE Hydrogen Program Review
NREL/CP-570-26938

TWO-PHASE FLOW CHARACTERISTICS IN FUEL CELLS AND ELECTROLYZERS

Hongtan Liu, Sadik Kakac and Lixin You
University of Miami
Coral Gables, FL 33124

Abstract

Two-phase flows are very important in both electrolyzers and fuel cell. A unified approach will improve our fundamental knowledge and provide a foundation for innovative designs of electrolyzers, fuel cells and reversible fuel cells.

In fuel cells, water is produced during electrochemical reactions. Since the membrane need water to keep high proton conductivity, and too much water will cause flooding, two-phase flow is a critical issue in fuel cells. It is very important to understand the two-phase flow characteristics in porous materials. In electrolyzers, bubbles formed need to transfer through the porous electrode to come out to the main flow stream. If bubbles can not be effectively removed from the reaction sites, the reaction rate will be limited. Thus it is very important to study the dependency of gas transfer rate on the properties of the porous electrodes.

As the first step, we developed single-phase models to study the effects of various parameters in fuel cell performance. In this model, general equations are developed for both the flow channel and the porous media. With a special technique, we do not need to provide the approximate boundary conditions at the interface; thus more accurate simulation results can be obtained. Since the feasibility of this approach has been verified, we have developed an initial two-phase flow model to study the two-phase flow characteristics in PEM fuel cells and electrolyzers.

A simple experimental setup has been built to study the mechanisms of gas transfer through liquid-filed porous media, as well as the effect of properties of porous gas diffuser on fuel cell performance.

1. Single-Phase Model-I

In this effort, we developed single-phase models to study the feasibility of the unified approach. Instead of modeling the different parts of the fuel cell sandwich separately, we developed models that can solve the governing equations in unified domains, so that no approximate boundary conditions are needed. This approach eliminates the errors introduced by the arbitrariness of the boundary conditions. The initial model development work started prior to this project. The first model we developed is a two-dimensional model for the entire fuel cell sandwich. In this model, the continuity equations, the momentum equations and the species concentration equations are solved in three different unified domains.

The reaction rate in the catalyst layer mainly depends on the reactant adsorption interaction with the catalyst and the active surface area of the catalyst. The adsorption rate in turn depends on the reactant concentrations in the catalyst layer, and thus depends on the concentrations at the interface between the diffusion layer and the gas channel. On the other hand, the concentrations at this interface depend on the reaction rate in the catalyst layer. At the time of when we started to develop our models, all the published models, either constant values or some predetermined variations of the concentrations were imposed at this interface. This obviously introduced some subjective arbitrariness.

In order to eliminate the arbitrary, or approximate boundary conditions, the governing equations (continuity equation, momentum equations, species concentration equations, and the electrochemical reaction equations) have to be solved in the unified domain consisting of the gas channels, the porous diffusion layers, the catalyst layers, and the membrane. The only independent variables for specified geometry and material should be the mass flow rates, temperature, humidity and the partial pressures of the species at the gas channel inlets, the external circuit resistance, and the temperature and flow rate of the cooling (or heating) agent. These are actually the parameters that can be controlled in real-life fuel cell operations or in laboratory experiments.

A special handling of the transport equations enabled us to use the same numerical method to solve them, and therefore to treat the gas channels, gas diffusers, catalyst layers and membrane as a single domain, avoiding arbitrary boundary conditions at their interfaces.

Since the model is involved, we will present only some typical results here. For the details of the model development and more results, please refer to our recent paper published in the ***AIChE Journal*** (Gurau et al. 1998).

1.1 Comparison with Experimental Results

Figure 1 is the comparison of computed fuel cell characteristic using the present model, with the experimental results of Ticianelli *et al.* (1988). It shows a very good agreement between the experimental work and our mathematical model.

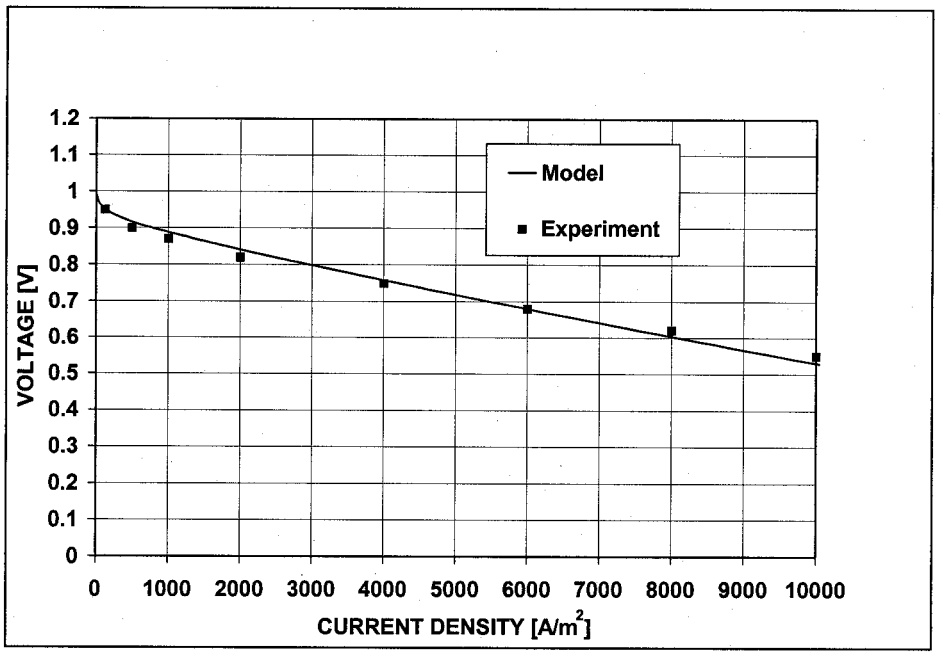

Figure 1. Comparison between the mathematical model and the experimental data (Gurau *et al.*, 1998)

1.2 Current Density

Figure 2 shows a typical result of current density variations along the flow direction. It can be seen that current density decreases along the flow direction, and the variation is not linear. If we had prescribed oxygen concentration boundary condition at the interface, the current density variation would then artificially mimic the boundary condition provided.

1.3 Effect of Porosity on Fuel Cell Performance

Figure 3 shows some typical result of polarization curve obtained by the model for different porosity of the diffusion layer. Note that the porosity have a very strong effect on the limiting current density. This result shows the importance of selecting appropriate diffusion layers. Please also note that, since this model is a single-phase model, no liquid water effects are considered. When two-phase flow is considered, the importance of the diffusion layer will be more pronounced especially the hydrophibicity effects.

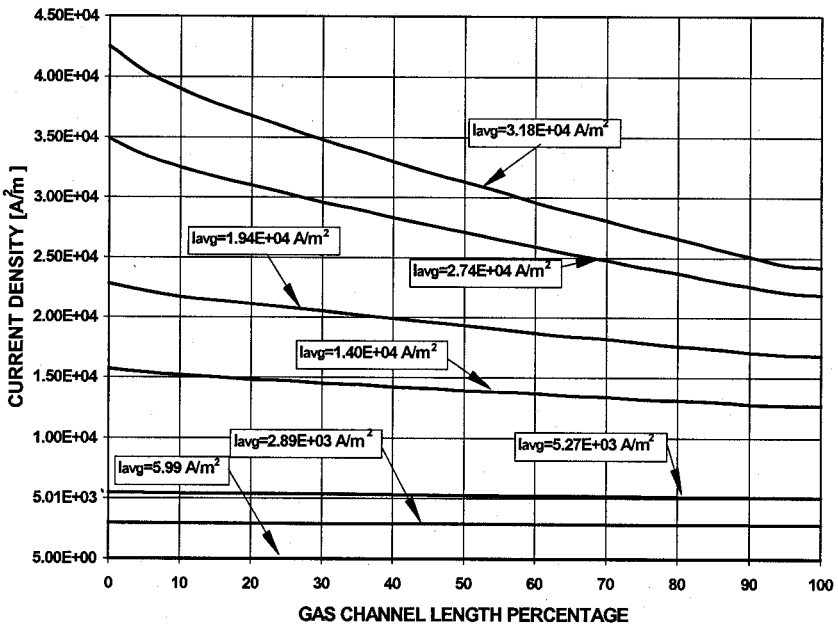

Figure 2. Current density variations along the flow direction at different average current densities (Gurau et al., 1998)

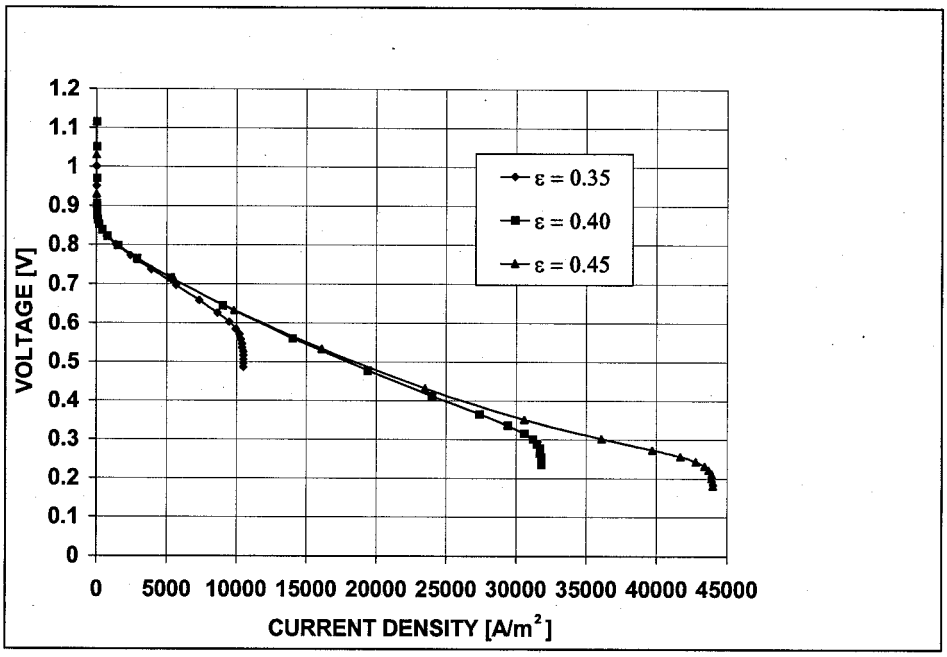

Figure 3. Some typical result of polarization curve obtained by the model for different porosity of the diffusion layer (Gurau et al., 1998)

2. Single-Phase Model-II

This model is developed mainly to study the effects of the third dimension and effects of different flow fields. This model is a two-dimension model: across the channel and across the fuel cell sandwich. The results of this model development have been reported in detail in a paper entitled "Modeling of Performance of PEM Fuel Cells with Conventional and Interdigitated Flow Fields," which has been accepted for publication the ***Journal of Applied Electrochemistry*** (Kazim et al., 1999). In the following, we present some of the typical results.

Figure 4 shows the modeling domain for both the conventional and the interdigitated flow fields. As shown in Fig. 4, the current collector is in contact with the porous diffusion layer between $x = L_1$ and $x = L_2$. At the interface of the gas diffuser with the gas channels, y=0, and at the interface between the gas diffuser and the catalyst layer $y = H$.

Figure 5 presents the progressive evolution of oxygen concentration in terms of different values of over-potential, η. Oxygen concentration remains constant only on the edge separating the gas-channel and the porous media, and reduces in the direction toward the reaction surface. Furthermore, as it was expected, low concentrations are obtained at points both located far away from the source of O_2 (namely at the boundary $L_1 < x < L_2$, $y = 0$) and on the reaction surface where the oxygen is chemically reduced ($0 < x < L$, $y = H$). The value of over-potential has a great effect on the oxygen concentration distribution, as was expected.

Figure 6 presents the evolution of oxygen concentration distribution in the gas diffusion layer of an interdigitated flow field. The same over-potential values as those used in the case results with conventional flow field are chosen to facilitate the comparison. The porous media now receives air only between $x = 0$ and $x = L_1$ at $y = 0$. With the new flow field design, the cathode gas stream flows through the porous media by forced convection rather than by diffusion.

Figure 7 shows the local current density $I(x)$ as a function of normalized variable x, for both conventional and interdigitated flow fields. Fig. 7 shows that the local current densities are much higher in the case of an interdigitated flow field.

The interdigitated flow field outperforms the conventional flow field especially at high current densities. When current density increases so does the oxygen consumption rate. The conventional flow field becomes quickly incapable of providing enough oxygen to satisfy its consumption. In the case of an interdigitated flow field, oxygen is transferred by forced convection, thus it can sustain much higher oxygen consumption rates. It can be seen from Fig. 8 that the limiting current density for a fuel cell with an interdigitated flow field is approximately three times that for a fuel cell with a conventional flow field. This is due to mass transfer enhancement in the interdigitated flow field. Figure 8 also shows that the maximum power density in the case of intersigitated flow field is doubled compared with the conventional flow field.

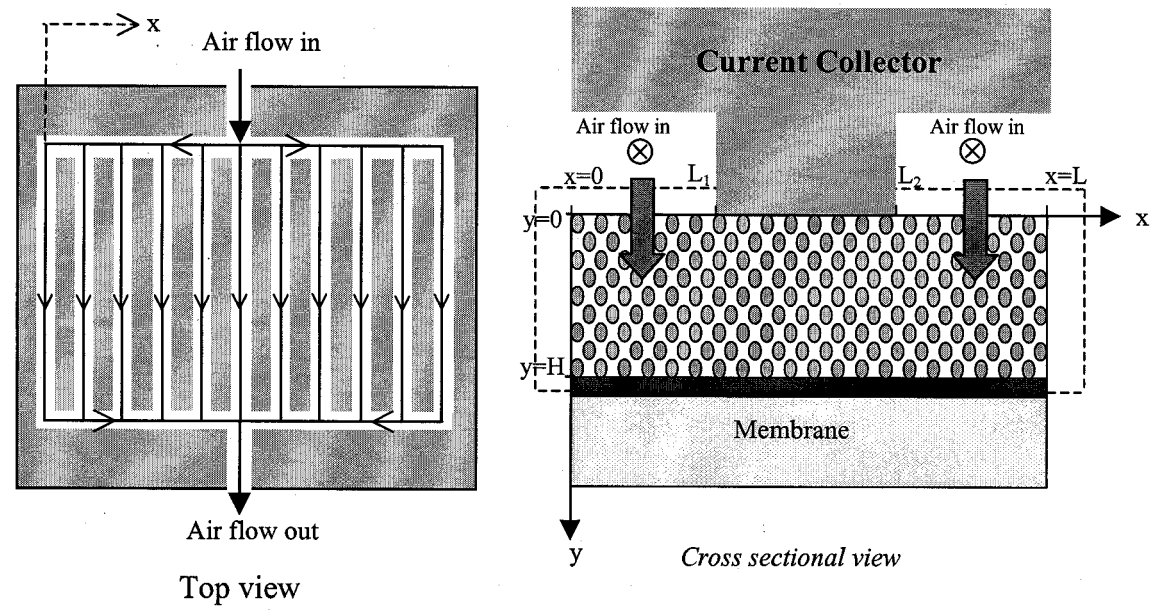

(a)

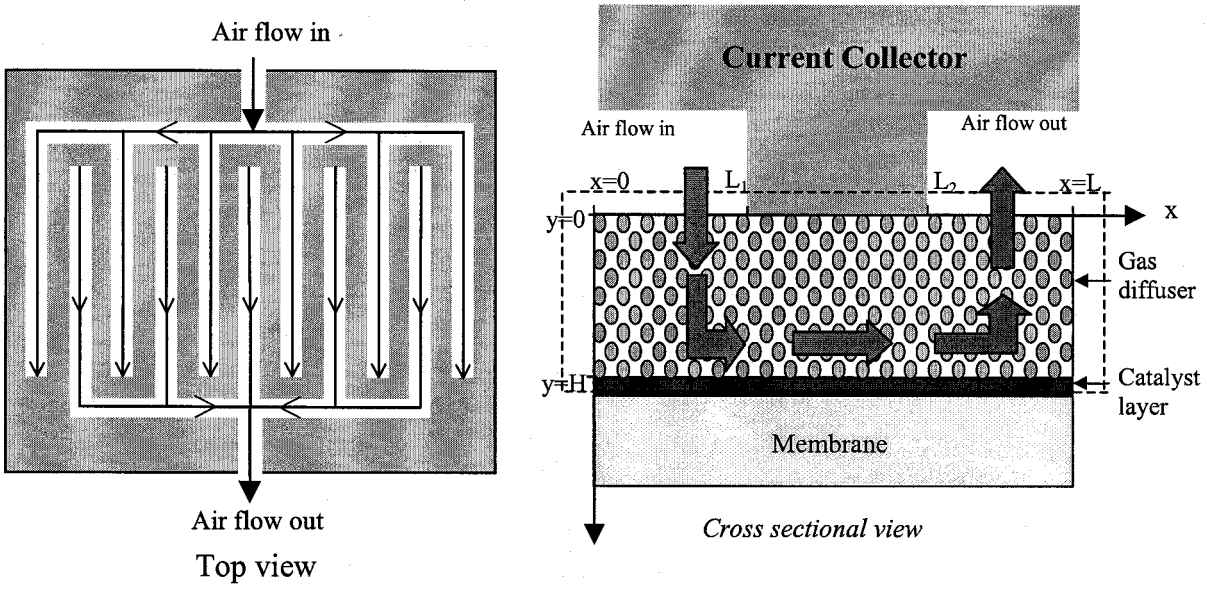

(b)

Figure 4. Schematic diagram of PEM fuel cell. (a) conventional flow field, (b) interdigitated flow field

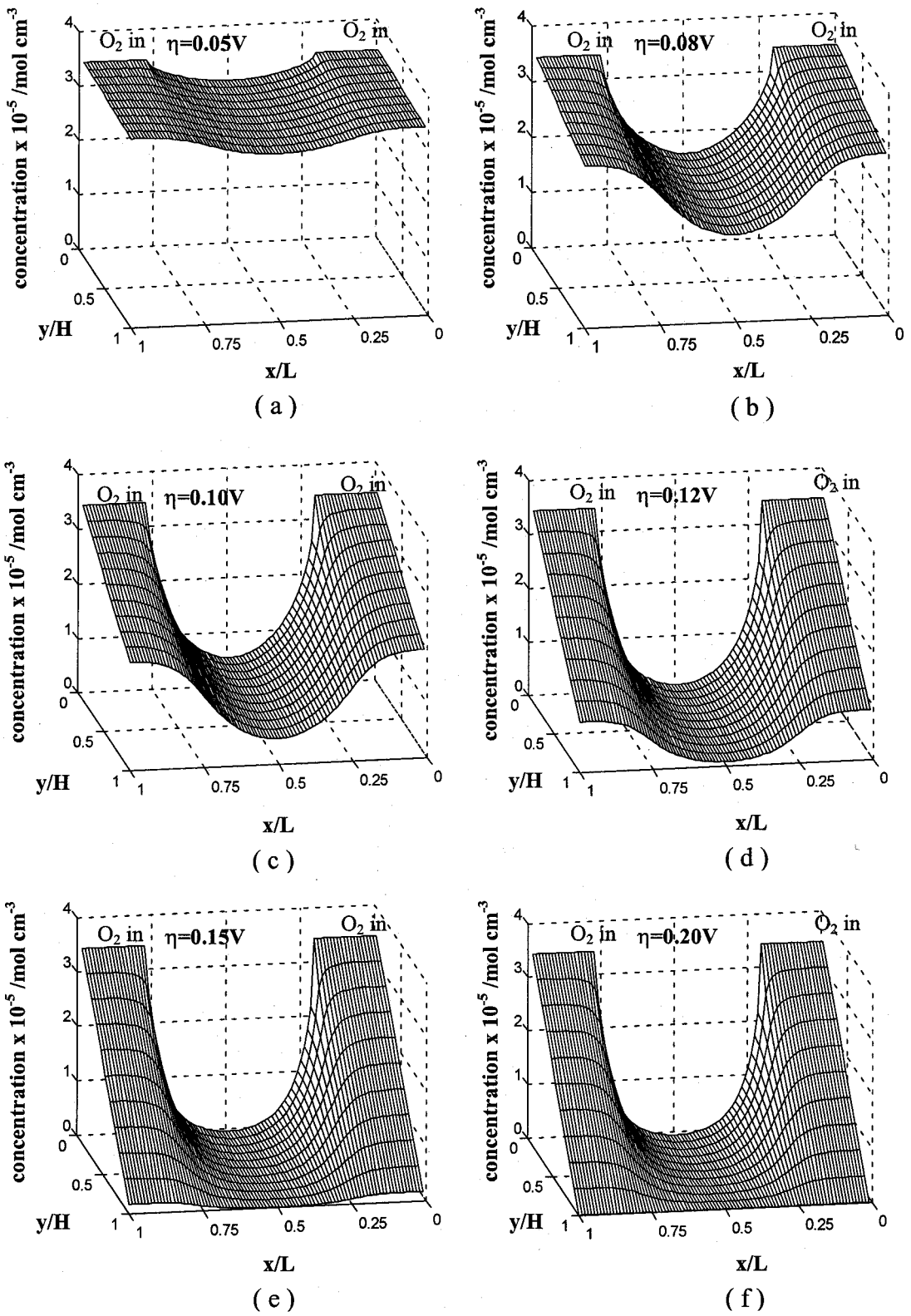

Figure 5. Oxygen concentration distribution in conventional flow field

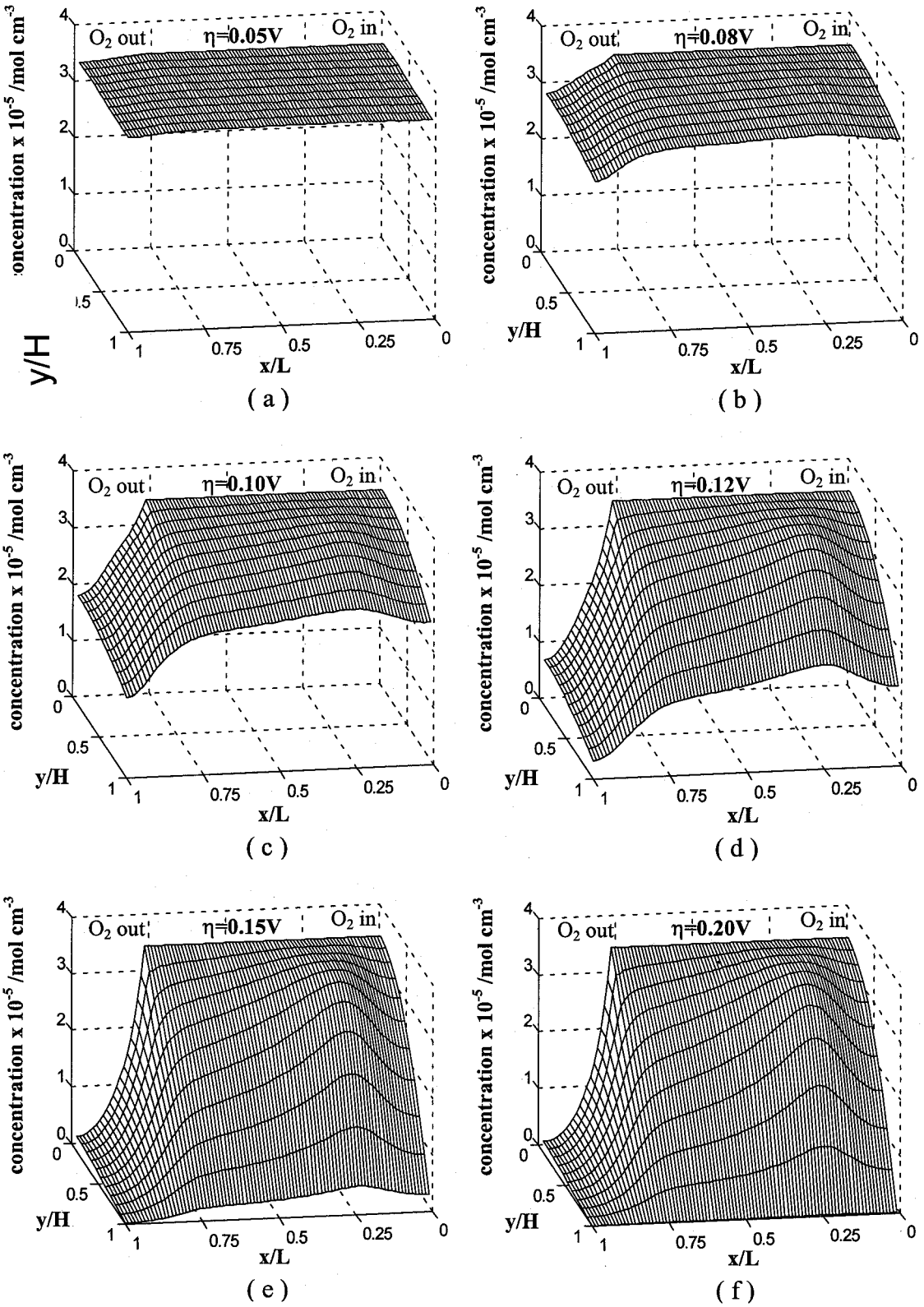

Figure 6. Oxygen concentration distribution in interdigitated flow field

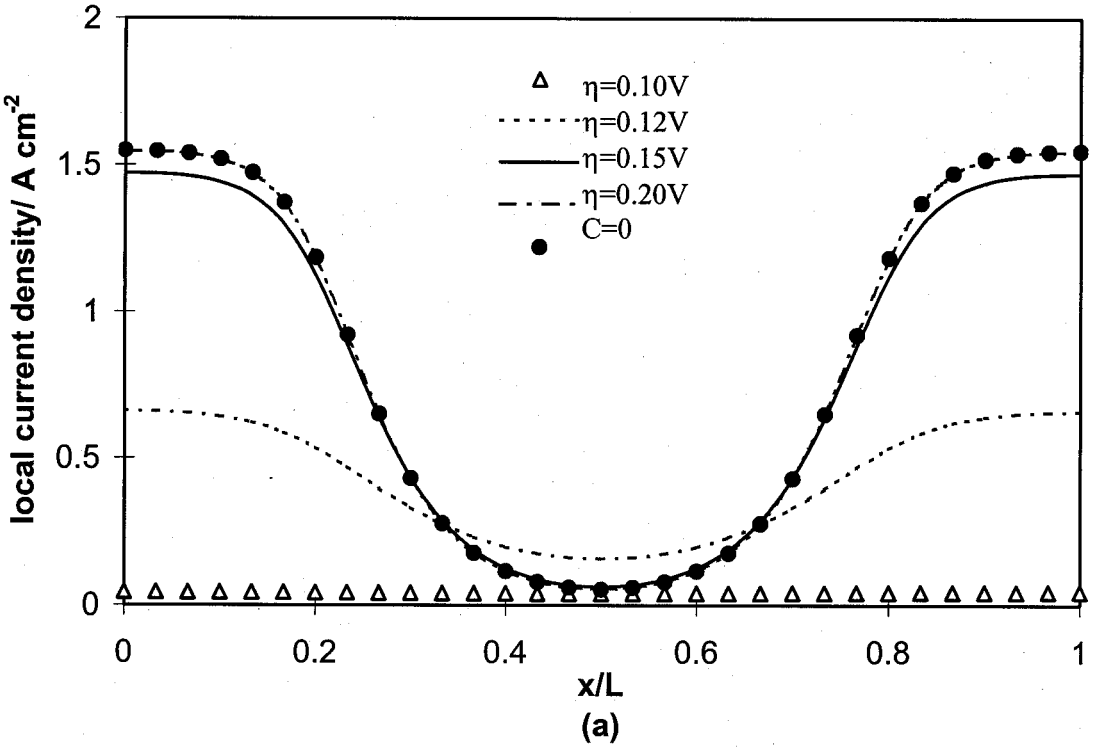

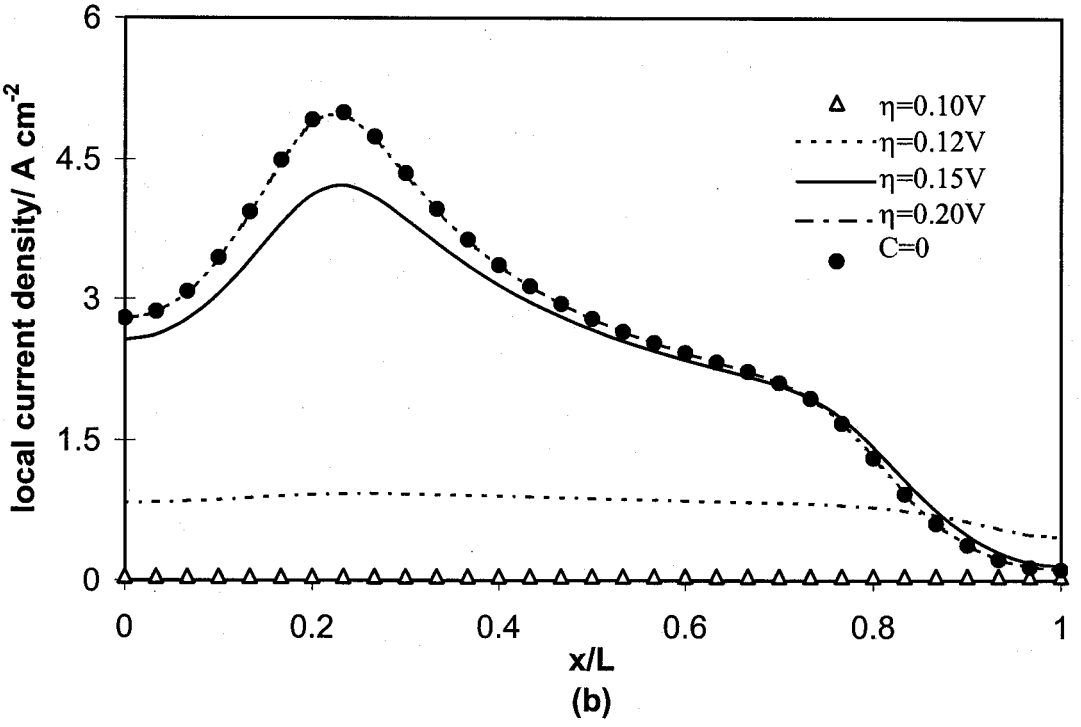

Figure 7. Polarization curves of fuel cells with conventional and interdigitated flow fields

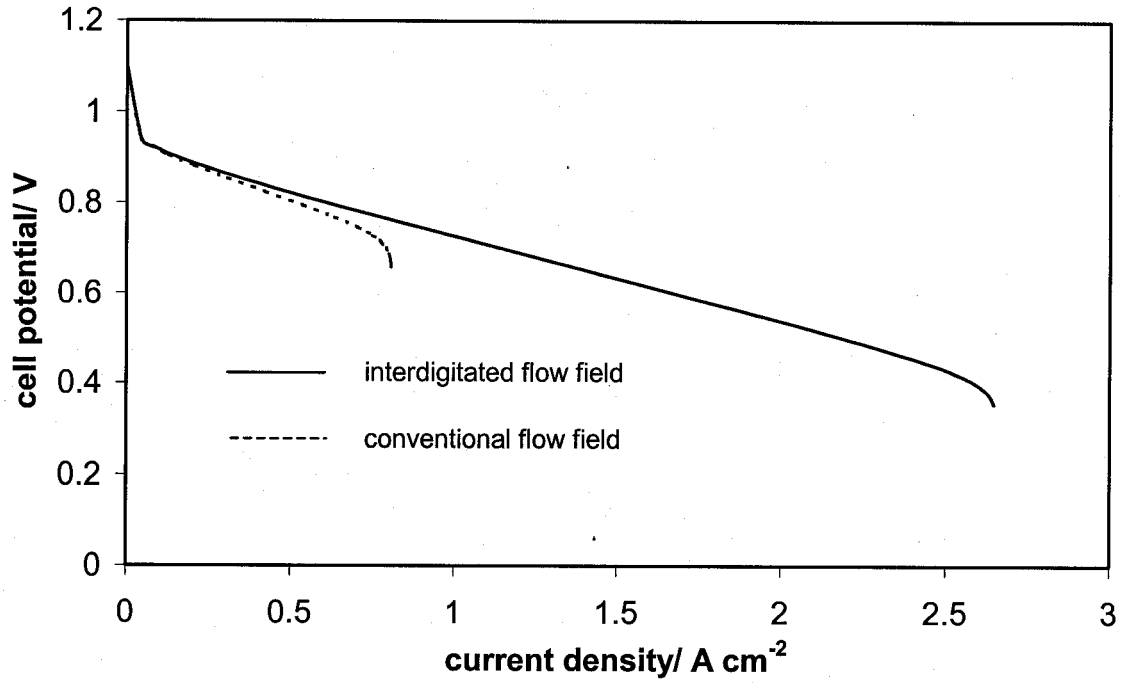

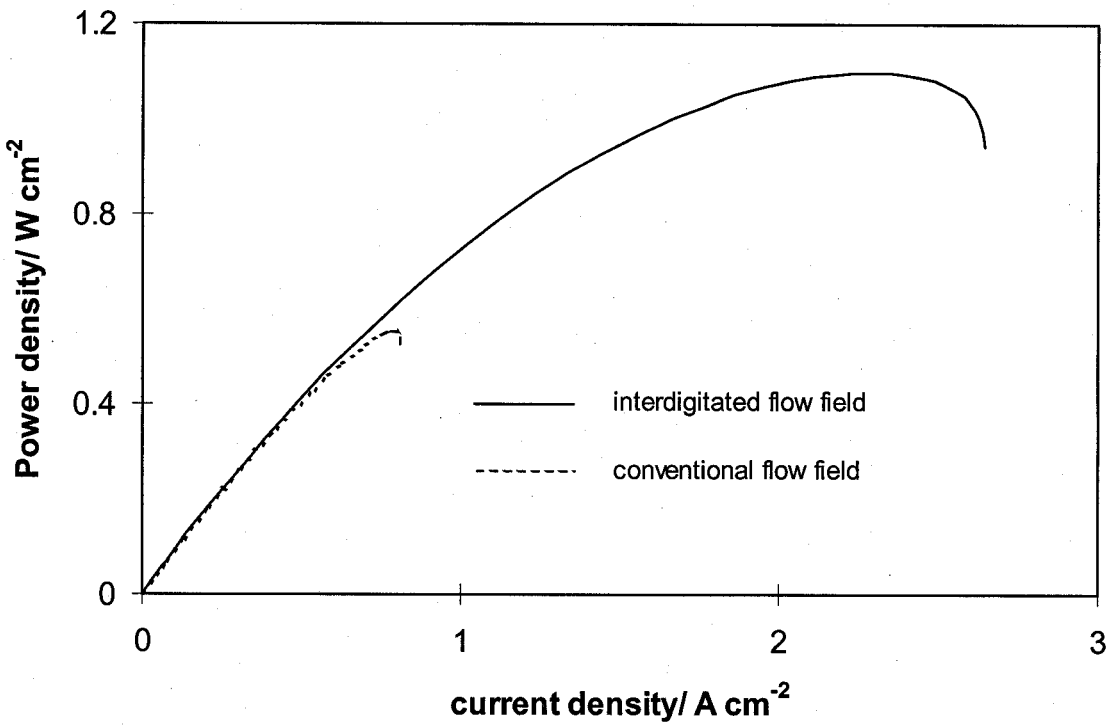

Figure 8. Comparison of polarization curves and power density of fuel cells with conventional and interdigitated flow fields

3. The Two-Phase Model

A two-phase mixture model is used to examine the two-phase flow field of hydrated air in the coupled flow channel and gas diffuser. The key idea in the multiphase mixture model is to focus on the level of a multiphase mixture, rather than on the levels of separate phases. In this model the multiple phases are regarded as constituents of a multiphase mixture. Multiphase flow can be described by a mass-averaged mixture velocity and a diffusive flux representing the difference between the mixture velocity and the individual phase velocity. In this definition, phases are assumed to be distinct and separable components with nonzero interfacial areas, and their mixture represents a single fluid with smoothly varying phase composition (Wang & Beckerman, 1993a, 1993b; Wang, 1997; Cheng & Wang, 1996; Wang & Cheng, 1996).

3.1 The Governing Equations for Two-Phase Mixture

A set of general conservation equations governing the transfer of a multiphase mixture has been developed in Wang and Cheng (1996). For a fuel cell or an electrolyzer, they can be expressed as in the following.

3.1.1 Continuity Equation. The mass conservation equation for a multiphase mixture can be readily be obtained by the addition of the individual phase conservation equation as

$$\varepsilon \frac{\partial \rho}{\partial t} + \nabla \cdot (\rho \vec{u}) = 0 \tag{1}$$

3.1.2 Momentum Conservation Equation. The coupled domain of gas channel and gas diffuser is studied in this paper. For the multiphase mixture in gas channel, the Navier-Stokes equation is applicable

$$\frac{\partial \vec{u}}{\partial t} + (\nabla \vec{u})\vec{u} = -\frac{1}{\rho}\nabla P + \nu \nabla^2 \vec{u} \tag{2}$$

For the multiphase mixture flow in the porous gas diffuser, the Darcy law can not be used because the diffuser is very thin, hence, both the velocity and velocity change across the diffuser are large, so the inertial force and viscous force can not be neglected here. For describing the multiphase mixture flow precisely, a generalized Darcy law is used

$$\frac{\partial \vec{u}}{\partial t} + (\nabla \vec{u})\vec{u} = -\frac{\varepsilon}{\rho}\nabla P + \nabla \cdot (\varepsilon \nu \nabla \vec{u}) - \frac{\nu}{K}(\varepsilon \vec{u}) \tag{3}$$

3.1.3 Species Conservation Equation. The species conservation equation for the multiphase mixture is

$$\varepsilon \frac{\partial}{\partial t}(\rho C^{\alpha}) + \nabla \cdot (\gamma_{\alpha} \rho \vec{u} C^{\alpha}) = \nabla \cdot (\varepsilon \rho D \nabla C^{\alpha}) + \nabla \cdot \left[\varepsilon \sum_k \left[\rho_k s_k D_k^{\alpha} (\nabla C_k^{\alpha} - \nabla C^{\alpha}) \right] \right] - \nabla \cdot \left[\sum_k C_k^{\alpha} j_k \right] \tag{4}$$

Because the domain volume in this paper is small and good cooling condition can be achieved, the isothermal condition is supposed in this preliminary research. We study two-phase flow problem here, so k=2 (liquid and gas phase), the α denote species, we consider oxygen, nitrogen and water respectively here. The mixture quantities in the above formulation are defined as

$$\rho = \rho_l s_l + \rho_g s_g \tag{5}$$

$$\rho\vec{u} = \rho_l \vec{u}_l + \rho_g \vec{u}_g \tag{6}$$

$$\rho C^\alpha = \rho_l s_l C_l^\alpha + \rho_g s_g C_g^\alpha \tag{7}$$

$$\rho D^\alpha = \rho_l s_l D_l^\alpha + \rho_g s_g D_g^\alpha \tag{8}$$

$$\upsilon = \frac{1}{\frac{k_{rl}}{\upsilon_l} + \frac{k_{rg}}{\upsilon_g}} \tag{9}$$

The correction factor γ_α in Equation (4) is given

$$\gamma_\alpha = \frac{\rho\left[\lambda_l C_l^\alpha + \lambda_g C_g^\alpha\right]}{\rho_l s_l C_l^\alpha + \rho_g s_g C_g^\alpha} \tag{10}$$

where the individual mobility λ_l, λ_g are

$$\lambda_l = \frac{k_{rl}/\nu_l}{k_{rl}/\nu_l + k_{rg}/\nu_g} \tag{11}$$

$$\lambda_g = \frac{k_{rg}/\nu_g}{k_{rl}/\nu_l + k_{rg}/\nu_g} \tag{12}$$

As in a traditional mixture theory, a diffusive mass flux of phase k within the two-phase mixture can be defined as

$$\vec{j}_k = \rho_k \vec{u}_k - \lambda_k \rho\vec{u} \tag{13}$$

$$\vec{j}_l + \vec{j}_g = 0 \tag{14}$$

$\vec{j}_l$ can be expressed as

$$\vec{j}_l = K\frac{\lambda_l}{\nu}\left(\nabla P - \nabla P_l\right) = K\frac{\lambda_l\lambda_g}{\nu}\nabla P_c \tag{15}$$

Once $\vec{j}_l, \vec{j}_g$ are solved, the individual phase velocities can be obtained from the mixture flow field by the following algebraic relations:

$$\rho_g \vec{u}_g = \vec{j}_g + \lambda_g \rho\vec{u} \tag{16}$$

$$\rho_l \vec{u}_l = -\vec{j}_g + \lambda_l \rho\vec{u} \tag{17}$$

3.1.4 Constitutive Relations

In this paper, the relative permeability for the liquid and gas phases is chosen to be represented by

$$k_{rl} = s_l^3 \tag{18}$$

$$k_{rg} = (1 - s_l)^3 \tag{19}$$

The two-phase capillary pressure can be expressed by a Leverett function $J(s_l)$ as follows (Wang & Cheng, 1996)

$$P_c = P_g - P_l = \sigma\left(\frac{\varepsilon}{k}\right)^{\frac{1}{2}} J(s_l) \tag{20}$$

$$\nabla P_c = \sigma\left(\frac{\varepsilon}{\kappa}\right)^{\frac{1}{2}} J'(s_l)\nabla s_l + \left(\frac{\varepsilon}{\kappa}\right)^{\frac{1}{2}} J(s_l)\left[\sum_{\alpha}\frac{\partial\sigma}{\partial C^{\alpha}}\nabla C^{\alpha} + \frac{\partial\sigma}{\partial T}\nabla T\right] \tag{21}$$

where

$$J(s_l) = 1.417(1 - s_l) - 2.120(1 - s_l)^2 + 1.263(1 - s_l)^3 \tag{22}$$

3.1.5 The Gas-Liquid Phase Equilibrium and the Species Equation Simplification

It is supposed that the oxygen and nitrogen can not dissolve in water in this paper because their solubility is very low, thus

$$C_l^{O_2} = 0,\ C_l^{N_2} = 0,\ C_l^{H_2O} = 1 \tag{23}$$

The water vapor partial pressure is the corresponding saturation vapor pressure at the local temperature (Springer et al, 1991)

$$\log_{10} P_v = -2.1794 + 0.02953T - 9.1837\cdot 10^{-5}T^2 + 1.4454\cdot 10^{-7}T^3 \tag{24}$$

the corresponding vapor density is

$$\rho_v^{H_2O} = \frac{P_v M}{RT} \tag{25}$$

thus, the concentration of water vapor in the gas mixture

$$C_g^{H_2O} = \frac{\rho_v^{H_2O}}{\rho_g} \tag{26}$$

For the oxygen

$$\rho C^{O_2} = \rho_g s_g C_g^{O_2} \tag{27}$$

Substitute the equation into Equation (4), we get,

$$\varepsilon\frac{\partial}{\partial t}\left(\rho C^{O_2}\right) + \nabla\cdot\left(\gamma_{O_2}\rho\vec{u}C^{O_2}\right) = \nabla\cdot\left(\varepsilon\rho D_g^{O_2}\nabla C^{O_2}\right) - \nabla\cdot\left(\frac{\rho}{\rho_g s_g}C^{O_2} j_g\right) \tag{28}$$

Similarly, for the nitrogen

$$\varepsilon\frac{\partial}{\partial t}\left(\rho C^{N_2}\right) + \nabla\cdot\left(\gamma_{N_2}\rho\vec{u}C^{N_2}\right) = \nabla\cdot\left(\varepsilon\rho D_g^{N_2}\nabla C^{N_2}\right) - \nabla\cdot\left(\frac{\rho}{\rho_g s_g}C^{N_2} j_g\right) \tag{29}$$

For the water:

$$\rho C^{H_2O} = \rho_g s_g C_g^{H_2O} + \rho_l s_l \tag{30}$$

$$\varepsilon \frac{\partial}{\partial t}\left(\rho C^{H_2O}\right) + \nabla \cdot \left(\gamma_{H_2O} \rho \vec{u} C^{H_2O}\right) = \nabla \cdot \left(\varepsilon \rho D_g^{H_2O} \nabla C^{H_2O}\right) - \nabla \cdot \left[\varepsilon \rho_l D_g^{H_2O} \nabla s_l\right] - \nabla \cdot \left[\left(\frac{\rho_v^{H_2O}}{\rho_g} - 1\right) j_g\right] \tag{31}$$

The two-phase mixture density is

$$\rho = \frac{s_g (P - P_v M^{H_2O})/(RT)}{C^{O_2}/M^{O_2} + C^{N_2}/M^{N_2}} \tag{32}$$

The gas mixture density is

$$\rho_g = \frac{1}{s_g}\left[\rho - \rho_l (1 - s_g)\right] \tag{33}$$

The gas and liquid phase saturation are respectively

$$s_g = \frac{\rho_l - \rho C^{H_2O}}{\rho_l - \rho_v^{H_2O}} \tag{34}$$

$$s_l = 1 - s_g \tag{35}$$

3.2 Boundary Conditions

The steady state is studied in this paper, so no initial conditions are required. At the inlet, the fluid is supposed to flow into the channel at uniform axial velocity. After a short flow passage, the velocity distribution across the channel section is nearly parabolic. So the standard exit boundary condition is supposed to exist at the right channel outlet. At the upper boundary, the vertical component of velocity is also supposed to be the standard exit, and the axial component of velocity is zero according to no-slip boundary condition (Schlichting, 1968). Both the vertical and axial component of velocity at the lower boundary are zero. For the species field, the inlet species concentration is supposed to be the known condition, no species exchange at the lower boundary and the right exit boundary is supposed. At the upper boundary, the oxygen concentration is supposed to be zero because of the electrochemical reaction. According to the above assumptions, the boundary conditions are

At x=0 (inlet):

$$u = u_{in},\ v = 0,\ C^{\alpha} = C_{in}^{\alpha}\ (0 \le y \le d_1) \tag{36}$$

$$u = 0,\ v = 0,\ \frac{\partial C^{\alpha}}{\partial x} = 0\ \ (d_1 \le y \le d_1 + d_2) \tag{37}$$

At x=l (outlet):

$$\frac{\partial u}{\partial x} = 0, \frac{\partial v}{\partial x} = 0,\ P = P_{ref},\ \frac{\partial C^{\alpha}}{\partial x} = 0\ (0 \le y \le d_1) \tag{38}$$

$$u = 0,\quad v = 0,\ \frac{\partial C^{\alpha}}{\partial x} = 0 \qquad (d_1 \le y \le d_1 + d_2) \tag{39}$$

At y=0

$$u=0, \qquad v=0\ , \frac{\partial C^{\alpha}}{\partial x}=0 \tag{40}$$

At $y=d_1+d_2$

$$u=0, \qquad \frac{\partial v}{\partial y}=0\ , \ C^{O_2}=0 \tag{41}$$

3.3 Governing Equations for Electrochemical Reaction in Catalyst Layer

The governing equations for describing the current distribution, potential distribution, oxygen flux and oxygen concentration in the catalyst layer are (Weisbrod & Vanderborgh)

$$\frac{dI_z}{dz}=A_v i_0^{+}\left\{\exp\left(\frac{\alpha_c F\eta}{RT}\right)-\exp\left(\frac{-\alpha_a F\eta}{RT}\right)\right\} \tag{42}$$

$$\frac{d\eta}{dz}=\frac{I_z}{\kappa_{\text{eff}}} \tag{43}$$

$$\frac{d(N_{O_2})}{dz}=-\frac{1}{4F}\frac{dI_z}{dz} \tag{44}$$

$$\frac{d(C_{O_2})_g}{dz}=-\frac{N_{O_2}}{D_{O_2}^{\text{eff}}} \tag{45}$$

where

$$i_0^{+}=i_0^{\text{ref}+}\left(\frac{C_{O_2}^{f}}{C_{O_2}^{\text{r,ref}}}\right) \tag{46}$$

3.4 Boundary Condition for the Catalyst Layer

At $z = 0$ (the interface of gas diffuser and catalyst layer)

$$I_z=0 \tag{47}$$

$$N_{O_2}=\frac{I_\delta}{nF} \tag{48}$$

$$C_{O_2}=C_{O_2}^{z=0} \tag{49}$$

At $z=\delta_c$ (the interface of catalyst layer and membrane)

$$\frac{d\eta}{dz}=\frac{I_\delta}{\kappa_\delta^{\text{eff}}} \tag{50}$$

3.5 Mathematical Model for the Membrane

The dimensions of membrane change with the water activity. Assuming that there is no excess volume of mixing between the ionomer and water, a relationship may be derived which describes the change in dimensions with water content. Molar concentration of water on a wet volume basis can be expressed as:

$$C_{H_2O}^{m,w} = \frac{a_d \lambda}{c_d \lambda + 1} \tag{51}$$

where

$$a_d = \frac{\rho_{m,d}}{E_m} \tag{52}$$

$$c_d = \frac{o_{m,d} M_w}{\rho_w E_m} \tag{53}$$

and λ represents water content in water molecules per sulfonate group, $\rho_{m,d}$ represents the density of the dry membrane, M_w the molecule weight of water, ρ_w the density of water, and E_m is the equivalent weight of the ionomer. Assuming that the membrane expands equally in all directions, the following relationship between wet and dry membrane thickness can be derived

$$z_{wet} = (c_d \lambda + 1)^{1/3} z_{dry} \tag{54}$$

Experiments conducted at Los Alamos have confirmed the equation (4). Experiments show that dimensional changes for NAFION 112 in both the machine and transverse directions generally yielded an increase of 18 to 21% in length, which compares favorably with a calculated value of 20% for NAFION with E_m=1100.

Water flux and concentration gradient through the membrane are desired. Therefore, the flux equation is solved for the concentration gradient and integrated through the membrane. Solution is facilitated by solving for λ, the molar ratio of water to sulfonate groups in the membrane, instead of water concentration. A generalized expression for species transport in moderately dilute solution is given by Newman as

$$N_i = \frac{-z_i D_i F C_i \nabla \phi}{RT} - D_i \nabla C_i - D_i C_i \nabla \ln a_{i,n} + C_i v \tag{55}$$

where

$a_{i,n}$ = activity of species i in solution

Since water is not charged, the first term in the equation (5) is zero. The second is diffusion term. The third term takes into account non-ideal solution behavior, which can be neglected here. The final term represents net transport because of bulk flow. If we assume that hydraulic permeability of the membrane is small, the last term can be neglected. Net movement of protons does induce water transport and is accounted for electro-osmotic drag, which will be presented later.

The diffusive water transport can be simplified as

$$N_{H_2O}^{diff} = -D_{H_2O} \nabla C_{H_2O} \tag{56}$$

For one-dimensional case

$$N_{H_2O}^{diff} = -D_{H_2O} \frac{dC_{H_2O}}{dz_{m,w}} \tag{57}$$

Since

$$\frac{dC_{H_2O}^{m,w}}{dz_{m,w}} = \left(\frac{dC_{H_2O}^{m,w}}{d\lambda} \right) \left(\frac{d\lambda}{dz_{m,w}} \right) \tag{58}$$

solving for the gradient in λ yields

$$\frac{d\lambda}{dz_{m,w}} = -\frac{N_{H_2O}^{diff}}{D_{H_2O}^{m,w}} \frac{1}{\left(\frac{dC_{H_2O}}{d\lambda} \right)} \tag{59}$$

Net water flux is the sum of diffusive transport and electro-osmotic drag as follows

$$N_{H_2O}^{net} = N_{H_2O}^{diff} + \frac{I_z n_d}{F} \tag{60}$$

After rearranging and substituting Eq.(10) into Eq.(9)

$$\frac{d\lambda}{dz_{m,w}} = -\frac{N_{H_2O}^{net} - \frac{I_{\delta_c} n_d}{F}}{D_{H_2O} \left(\frac{dC_{H_2O}}{d\lambda} \right)} \tag{61}$$

Introducing the following non-dimensional parameters

$$N_i^* = \frac{N_i}{N_{H^+}} \tag{62}$$

$$N_{H^+}^* = \frac{I_{\delta_c}}{F} \tag{63}$$

$$\xi_{m,d} = \frac{z_{m,d}}{\delta_{m,d}} \tag{64}$$

Eq.(11) can be expressed as non-dimensional form

$$\frac{d\lambda}{d\xi_{m,d}} = -\frac{\delta_{m,d} I_{\delta_c} \left(N_{H_2O}^* - n_d \right) (c\lambda + 1)^{1/3}}{D_{H_2O} F \left(\frac{dC_{H_2O}}{d\lambda} \right)} \tag{65}$$

At the interface of the ionomer, the water concentration depends on the water activity (Zawodzioski et al)

$$\lambda = 0.043 + 17.81a - 39.85a^2 + 36.0a^3 \quad \text{for } (0 < a \le 1) \tag{66}$$

$$\lambda = 14.0 + 1.4(a - 1) \quad \text{for } (1 < a \le 3) \tag{67}$$

$$\lambda = 16.8 \quad \text{for } (a \ge 3) \tag{68}$$

$$\lambda = 22. \quad \text{if liquid water exists} \tag{69}$$

where a is the water activity

$$a = \frac{x_w P^t}{P_{sat}} \tag{70}$$

The water diffusion coefficient in ionomers for Nafion 117 can be expressed as

$$D_{H_2O} = \left(-1.102 + 9.129\left(1 - \exp\left(-0.108\lambda\right)\right)\right)\left[\frac{E_a}{R}\left(\frac{1}{303} - \frac{1}{273+T}\right)\right] \tag{71}$$

For Nafion 117, the ionic conductivity can be expressed as

$$\kappa_i = (-4.43 + 0.0179T)\{-0.0108 + 0.2365[1 - \exp(-0.0285\lambda)]\} \tag{72}$$

The membrane resistance AR_m is calculated by integrating over the membrane thickness by the following equation

$$AR_m = \int_0^{\delta_m} \frac{dz_w}{\kappa(\lambda)} = \int_0^{\delta_m} \frac{(c_d\lambda + 1)^{1/3} dz_d}{\kappa(\lambda)} \tag{73}$$

3.6 Fuel Cell Performance

Cell voltage is calculated as

$$V = V_{oc} - I \cdot AR_m - \eta_c\Big|_{z=\delta_c} - \eta_{con} \tag{74}$$

where V_{oc} is open circuit voltage, I is current density, η_c is the activation over-potential, η_{con} is concentration overpotential, AR_m is membrane resistance(23).

$$V_{oc} = 0.0025T + .2329 \tag{75}$$

$$\eta_{con} = -\frac{RT}{nF}\ln\left(\frac{C_S}{C_B}\right) \tag{76}$$

where C_B is bulk concentration, C_S is surface concentration.

3.7 Numerical Procedures

The Navier-Stokes equation for the fluid channel and the generalized Darcy equation for the porous medium are solved by numerical methods. The two equations can be expressed as the following general form

$$(\nabla u)\vec{u} = \nabla \cdot (\Gamma \nabla u) + S - \frac{1}{\rho}\nabla P \tag{77}$$

where S is source term. For the fluid layer, S=0; For the porous layer,

$$\mathrm{S} = -\varepsilon\frac{\nu}{\mathrm{K}}\mathrm{u} \tag{78}$$

The source term in the general equation does not include the pressure term because the pressure field is of interest.

For the species equation, the oxygen and water equation (27) and (30) are solved. The nitrogen concentration can be obtained by

$$C^{N_2} = 1 - C^{O_2} - C^{H_2O} \tag{79}$$

The convection and diffusion terms in the species equation are similar to the momentum equation, other terms in the species equation caused by the interphase flux and phase change can be dealt with as source terms in the general differential equations.

The general differential equations are discretized by the control-volume based finite difference method of Patankar (1980), and the resulting set of algebraic equations are iteratively solved. The solutions of velocity component of the equations are obtained in a staggered control volume, see Patankar (1980) for details. In addition, there exists a fundamental difficulty in the calculation of the velocity field as related to the pressure gradient. This is overcome by the so-called the Semi-Implicit method for Pressure-Linked Equations Revised (SIMPLER) algorithm developed by Patankar(1980).

The rectangular physical domain is divided by a uniform grid consisting of n vertical gridlines in the axial direction and by a non-uniform grid consisting of m1 horizontal grids in the fluid channel and (m-m1) gridlines in the porous layer in the vertical direction. Stringent numerical tests were performed in every case to ensure that the solutions were independent of the grid size. For the examples to be illustrated below, it was found that the typical number of gridlines along the axial direction was 60, while a similar number of gridlines was needed along the vertical direction in 2-dimensional tests. The convergence is considered to be reached when the solution is stable, both the sum of absolute mass source of every control volume and the absolute errors of the sum of the species concentration for all control volumes between two consecutive iterations are less than 0.005.

The governing equations in the catalyst layer are a two-point boundary problem that can be solved by relaxation method.

3.8 Model Predicted Results and Discussions

3.8.1 The Influence of Water Influx at the Boundary

Figure 9 and 10 show the oxygen, nitrogen and water vapor concentration field and liquid and gas phase flow field respectively when the inlet gas velocity u=0.035m/s and water flow in at the boundary. The inlet gas concentrations is $C^{H_2O} = 0.47$, $C^{O_2} = 0.12$. Figure 9a shows the oxygen concentration field. The oxygen concentration decreases towards the boundary because electrochemical reaction occurred at the boundary (catalyst layer). It is shown that oxygen has a large concentration gradient. It is because the gas velocity is low, the influence of convection is low and the concentration field is dominated by the diffusion. Figure 9b shows the water vapor concentration is higher at the catalyst boundary than at the diffuser-channel boundary. Figure 9c shows the nitrogen concentration increases toward the boundary, and the concentration gradient is also large, which can be easily accounted by the mass counter diffusion theory.

Figure 10a shows the liquid water flow field in the gas diffuser. At the inlet of the gas diffuser, liquid water flows into the diffuser from the channel, the velocity is relatively large, this is accounted for the isothermal model in this paper. The air in PEM fuel cell

must be usually hydrated at elevated temperature to increase water content, and hence to increase the water content in the membrane. When the high temperature hydrated air enters the lower temperature fuel cell, superheated vapor will condense into water. So the water has a large velocity at the inlet. In the bulk of gas diffuser, the liquid water flow field will be governed by the inlet water condensed from the vapor and by water influx at the boundary. From the figure, it is shown that the water velocity field is dominated by the production of water due to the electrochemical reaction near the catalyst boundary and by the inlet vapor condensation in the inner part of the gas diffuser respectively. Most water will flow out from the diffuser at the right boundary and will be carried away by the main gas stream in the channel.

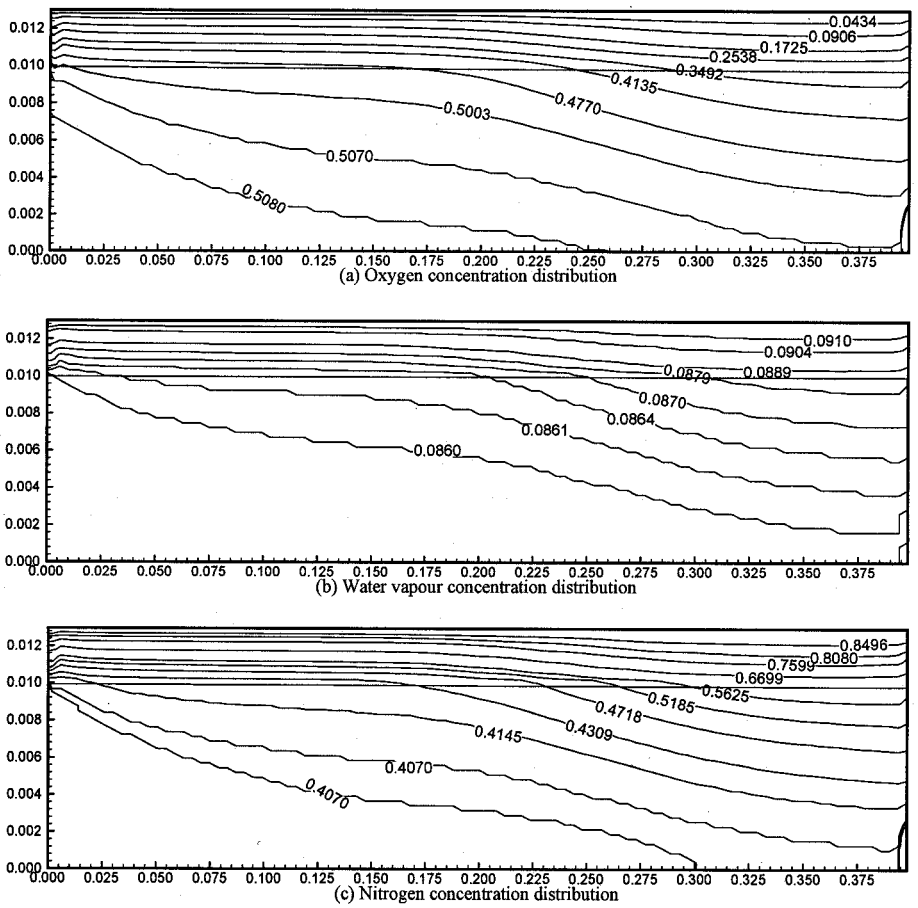

Figure 9. The species concentration field when water flow in the diffuser

Figure 10b shows the gas flow field in the gas diffuser. The gas velocity is generally low due to the low velocity of inlet gas stream in the channel. At the left boundary, the gas flows into the diffuser at a large vertical velocity. The oxygen will be consumed at the catalyst layer boundary; superheated vapor will condense to liquid water. The vapor and liquid water can interchange in the diffuser depending on the local vapor pressure and temperature. The main velocity component in the diffuser is horizontal. There exists a

large velocity gradient across the porous diffuser. At the upper boundary the velocity is zero according to no-slip boundary condition. At the interface of the gas diffuser and the channel, the interface velocity on the side of the gas diffuser is much bigger than the upper boundary, but it is not continuous with the interface velocity on the side of flow channel. The difference between these two interface velocities is called slip velocity. The slip velocity depends on various factors, such as the relative width of the gas diffuser, the porosity, the permeability of fluid in the porous diffuser and the Reynolds number.

The existence of fluid velocity in the porous diffuser has various influences on the flow field and the mass transfer. At first, the existence of velocity surely influences the mass transfer, so some previous fuel cell models which consider only the mass transfer induced by the concentration gradient are not reasonable. In addition, both the gas velocity and velocity change across the porous diffuser are large because the width of the porous diffuser is relatively thin in the fuel cells. Thus the Darcy law can not be used to describe the flow field in the diffuser, a generalized Darcy law is necessary to describe the flow field in the gas diffuser as presented in Equation (3).

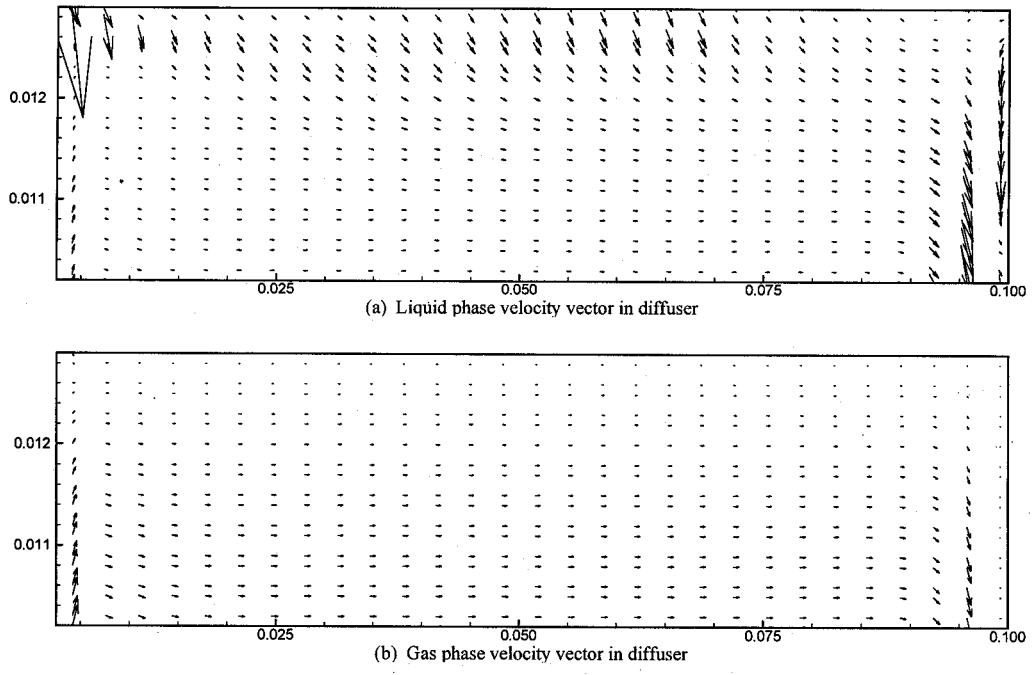

(a) Liquid phase velocity vector in diffuser

(b) Gas phase velocity vector in diffuser

Figure 10. The two-phase flow field when u=0.035m/s and water flow in *The Influence of the Water Outflux at the Boundary*

When the current density is small, water may flow out of the diffuser. Figure 11 show the liquid and gas flow field when the inlet gas velocity u_{in}=0.1m/s. The inlet gas concentrations in Figure 11 are: $C^{H_2O} = 0.47$, $C^{O_2} = 0.22$. In contrast with flow field in Figure 10, the liquid water flow toward fluid channel.

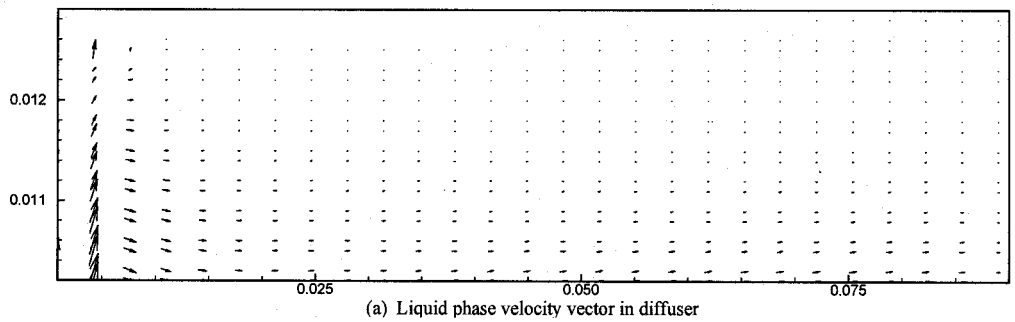

(a) Liquid phase velocity vector in diffuser

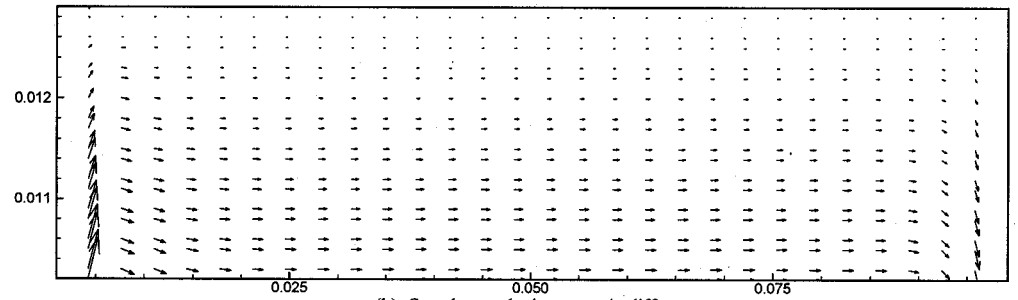

(b) Gas phase velocity vector in diffuser

Figure 11. The two-phase flow field when $C^{H_2O} = 0.47$, $C^{O_2} = 0.22$ and water flow out

Two-phase mixture model has been successfully used to predict the two-phase flow in the PEM fuel cell gas diffuser. A set of the governing equations for the two-phase flow in the PEM fuel cell gas diffuser was derived, various influencing factors on the two-phase flow field are discussed. The predicting results of the two-phase flow are presented. The predicting results show that inlet gas species concentration (especially vapor concentration), inlet gas velocity and water flux boundary condition all combine to influence the two-phase flow. After the two-phase flow field in the gas diffuser is known, it is possible to propose the optimum schemes for water management in the PEM fuel cells.

4. Experimental Setup

A simple experimental system for two-phase flow in porous media has been constructed, and it is shown schematically in Figure 12. The setup will be used to study the effects of various parameters on the two types of two-phase flows in porous media encountered in fuel cells and electrolyzers.

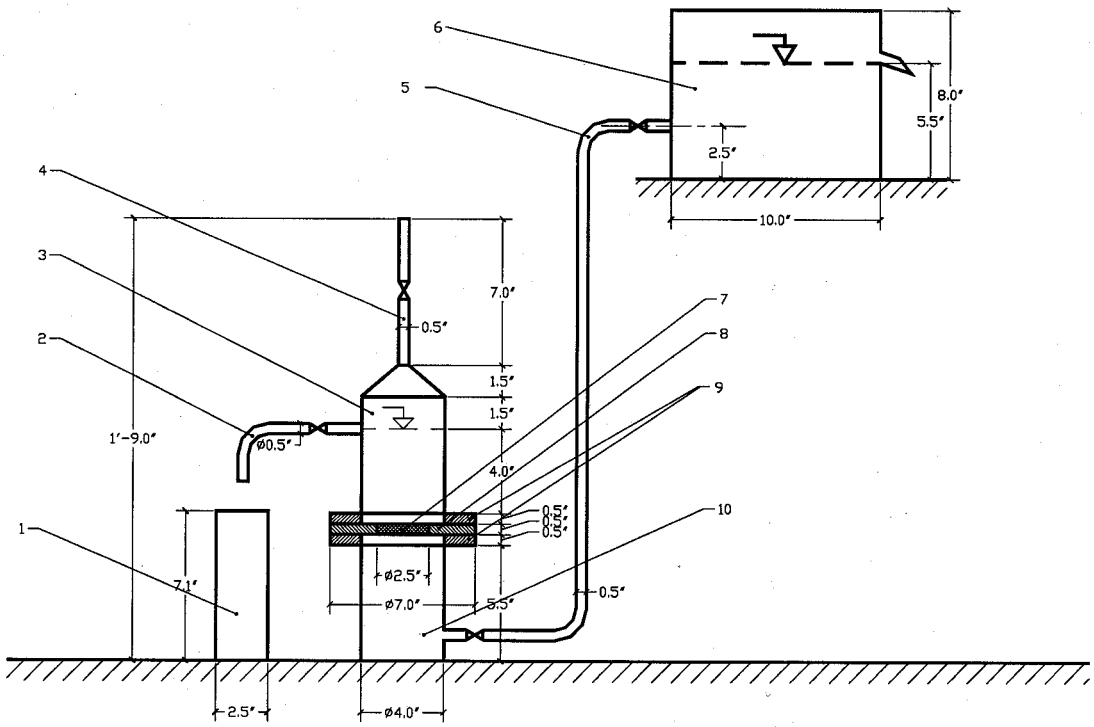

1. Graduated cylinder (transparent)
2. Tube
3. Container (transparent)
4. Tube
5. Tube
6. Water tank
7. Porous medium
8. Flange
9. Flange
10. Container

Figure 12. Schematic of the experimental setup for two-phase flows in porous media

References

Abriola, L. M. & Pinder, G. F.(1985), A multiphase approach to the modeling of porousmedia contamination by organic compounds 1. Equation development, II. Numerical simulation, *Water resources research,* (**21**),11-26

Bernardi, D. M. & Verbrugge, M. W.(1991), Mathematical model of a gas diffusion electrode bonded to a polymer electrolyte, *AIChE Journal*, (**37**), 1151-1163

Bernardi, D. M. & Verbrugge, M. W.(1992), A mathematical model for the solid-polymer-electrode fuel cell. *J. Electrochem. Soc.*,(**139**), 2477-2491

Cheng, P. & Wang, C. Y., (1996), A multiphase mixture model for multiphase, multicomponent transport in capillary porous media -- II: numerical simulation of the transport of non aqueous phase liquids in the unsaturated subsurface, *Int. J. Heat Mass Transfer*,(**39**), 3619-3632

Gurau, V., Liu, H.T. & Kakac, S., (1998), Two-dimensional model for Proton Exchange Membrane fuel cells, AIChE Journal, (44), 2410-2422

Kazim, A., Liu, H. T. & Forges, P., Modeling of Performance of PEM Fuel Cells with Conventional and Interdigitated Flow Fields, J. of Applied Electrochemistry, accepted.

Mosdale, R. & Srinivasan, S. (1995), Analysis of performance and of water and thermal anagement in PEM fuel cells, *Electrochemica Acta*, (**40**), 413-421

Rho,Y. W. & Srinivasan, S. (1994), Mass transport phenomenona in PEM fuel cells using O_2/He, O_2/Ar and O_2/N_2 mixtures, *J. Electrochem. Soc.*,(**141**),2089-2096

Patankar, S. V., (1980), *Numerical heat transfer and fluid flow*, Hemisphere, Washington, D. C.

Schlichting, H., (1968). *Boundary layer theory*, 6th ed., McGraw-Hill, New York, 367-383.

Springer, F. E. , Zawodzinski, T. A. & Gottesfeld, S.(1991), Polymer electrolyte fuel cell model, *J. Electrochem. Soc.*,(**138**), 2334-2342

Wang, C. Y. & Beckermann, C. (1993a), A two-phase mixture model of liquid-gas flow and heat transfer in capillary porous media Part I: formulation, *Int. J. Heat Mass Transfer*, (**36**), 2747-2758.

Wang, C. Y. & Beckermann, C.(1993b), A two-phase mixture model of liquid-gas and heat transfer in capillary porous media Part II: application to pressure-driven boiling flow adjacent to a vertical heated plate, *Int. J. Heat Mass Transfer*, (**36**), 2759-2768

Wang, C. Y.(1997), A fixed-grid numerical algorithm for two-phase flow and heat transfer in porous media, *Numerical Heat Transfer B, Fundamentals*, (**31**),85-105

Wang, C. Y. & Cheng, P.(1996), A multiphase mixture model for multiphase, multicomponent transport in capillary porous media -- I: model development, *Int. J. Heat Mass Transfer*,(**39**),3607-3618

Watanabe, M., Satoh, Y. & Shimura, C.(1993), Management of the water content in polymer electrolyte membranes with porous fiber wicks. *J. Electrochem. Soc.*,(**140**), 3190-3193

Weisbrod, K. R., Grot, S. A. & Vanderborgh, N., Through-the-electrode model of a Proton Exchange Membrane fuel Cell. Proc. of 1st Int. Sym. on Proton Conducting Membrane fuel cells, Vol95-23, The Electrochemical Society, 1995

Zawodzinski, T. A.(1993), Water uptake by and transport through Nafion 117 membrane, *J. Electrochem. Soc.*, (**140**), 1041-1047

List of Figures